Design and performance of a microsecond time-resolved photo-chemically induced dynamic nuclear polarization add-on for a high-field nuclear magnetic resonance spectrometer

I. Kuprov
Department of Chemistry, University of Oxford, Physical and Theoretical Chemistry Laboratory, South Parks Road, Oxford OX1 3QZ, United Kingdom

M. Goez
Fachbereich Chemie, Martin Luther Universität Halle-Wittenberg, Kurt-Mothes-Strasse 2, D-06120 Halle/Saale, Germany

P. A. Abbott and P. J. Hore[a)]
Department of Chemistry, University of Oxford, Physical and Theoretical Chemistry Laboratory, South Parks Road, Oxford OX1 3QZ, United Kingdom

(Received 1 June 2005; accepted 9 July 2005; published online 12 August 2005)

We describe the design and operation of microsecond time-resolved photo-chemically induced dynamic nuclear polarization hardware, designed to go with a commercial 600 MHz nuclear magnetic resonance (NMR) spectrometer. A frequency-tripled neodymium-doped yttrium/aluminum garnet (Nd:YAG) laser is used as the light source, with a system of mirrors or prisms to route light to the NMR sample from above, removing the need for NMR probe modifications. The experiment has been designed for a shared NMR spectrometer and is straightforward and inexpensive to assemble and operate. © *2005 American Institute of Physics.* [DOI: 10.1063/1.2010287]

I. INTRODUCTION

Chemically induced dynamic nuclear polarization (CIDNP) is the name given to the nonequilibrium nuclear spin level populations produced in chemical reactions that proceed through radical pair intermediates.[1,2] CIDNP is manifested as enhanced nuclear magnetic resonance (NMR) absorption or emission (net effect) and distortion of the relative intensities of multiplet components (multiplet effect).[3] The magnitude and sign of the polarization are determined by the magnetic properties and kinetics of the radical reaction intermediates.[1–3] The theory of CIDNP is well developed and allows extraction of radical reaction rate constants, hyperfine couplings, *g* values, and nuclear paramagnetic relaxation rates from experimental data.[4,5] The primary applications of this phenomenon, and in particular of its photoinduced variant (photo-CIDNP), have been investigations of radical reaction mechanisms[1–3] and structural studies of proteins.[6–8] The latter rely on the fact that tyrosine, tryptophan, and histidine amino acid residues can be polarized using a photosensitizer, and the existence of the polarization implies that the residue is located on the surface of the protein, exposed to bulk solvent.[8] Photochemical NMR experiments in general are not restricted to photo-CIDNP studies and include, among others, photochemical cage release experiments,[9,10] macromolecular folding studies,[11] investigations of photochemical kinetics,[12–14] and studies of photoactive proteins.[15–18]

The two main experimental techniques for photo-CIDNP NMR are the continuous-wave (cw) and time-resolved methods. cw photo-CIDNP is generally more popular, not least because it is relatively straightforward to implement using ultraviolet (UV) lamps[19] or cw lasers together with fiber optics.[20,21] Prolonged irradiation of NMR samples can also lead to strong polarizations, with 20- to 50-fold magnetization enhancements being quite common.[22] However, with illumination times of 50–5000 ms, a cw photo-CIDNP experiment detects a time-averaged or steady state value of the photochemically generated magnetization, which yields mechanistic information, but precludes kinetic studies.

The time-resolved photo-CIDNP technique, using a pulsed laser as the light source, is best suited for exploring events on a microsecond to millisecond timescale in photoinduced spin-selective reactions.[12,14,23] Time-resolved photo-CIDNP experiments generally require light pulses much shorter than 1 μs and pulse energies of at least 50 mJ. The resulting incident optical power densities are incompatible with optical fibers and rule out the use of illumination schemes that have been developed in the more mainstream cw CIDNP and optical NMR field.[10,20]

The pioneering work by Miller and Closs[24] a quarter of a century ago described a time-resolved photo-CIDNP installation based on an electromagnet 60 MHz Fourier transform (FT) NMR spectrometer, in which the laser- and rf-control electronics were custom made and, of necessity, rather complex, but light routing was straightforward because the coil region of the probe was easily accessible from outside the magnet.[25] With the introduction of superconducting magnets the geometry around the sample volume has become much more constrained and difficult to access, such that sample

[a)]Author to whom correspondence should be addressed; electronic mail: peter.hore@chem.ox.ac.uk

irradiation can require, at the very least, "moving a few capacitors and drilling a few holes" in the probe,[6] and sometimes also sacrificing one of the probe rf coils for synchronization purposes.[26] Hitherto, the method of choice for high-field time-resolved CIDNP studies has been to use a ≈ 5 mm diameter, cylindrical fused silica light guide passing off axis through the body of the NMR probe, surmounted by a prism to bring the light into the NMR sample from the side through a window in the radiofrequency (rf) coil.[6,7,27] Another popular variant has the light guide on axis, bringing light from below into the sample contained in a flat-bottommed NMR tube. In both cases, probe hardware modifications are inevitable.[6] Routing light from below has also become more difficult because the sophisticated and fragile temperature-control equipment needs to be relocated. Even if the latter can be achieved, the resulting axial asymmetry leads to field homogeneity distortions. Moreover, such probe modifications normally invalidate the manufacturer's warranty. With cryoprobes gaining in popularity, it is becoming obvious that "do-it-yourself" probe modification is no longer an attractive option, except for highly specialized applications.

The requirements for a modern time-resolved CIDNP installation are: low cost, ease of assembly, use of readily available commercial components, and compatibility with multiuser high-field NMR spectrometers without the need for the modification of either probes or rf and synchronization circuitry. All of this has gradually become possible in recent years with the appearance of powerful and flexible pulse programming languages and commercial lasers with built-in TTL synchronization lines, thus eliminating the need for constructing the more complicated parts of the Miller and Closs design.[24]

We describe here the design and operation of a time-resolved photo-CIDNP system recently developed in Oxford, based on a frequency-tripled neodymium-doped yttrium/aluminum garnet (Nd:YAG) laser and a shared 600 MHz NMR spectrometer equipped with multiuser probes that could not be modified to permit sample irradiation. The utility of the approach is not restricted to photo-CIDNP measurements, other applications being microsecond time-resolved studies of photochemical reactions[12–14] and photo-induced transformations of biomolecules.[11,15–18]

II. TIME-RESOLVED CIDNP HARDWARE: GENERAL CONSIDERATIONS

A. Light routing

The main challenge in designing time-resolved CIDNP hardware is efficient and robust light routing. To preserve the magnetic field homogeneity, the laser cannot be brought closer to the superconducting magnet than about 1.5 m. The entrance to the magnet bore is 2 m or more above floor level, and the sample, in the center of the magnet, is more than 1 m below the top of the bore. Modern NMR magnets are suspended on air bearings, which are normally sufficiently stable to keep the horizontal drift below 0.5 mm day, the primary cause of drift being changes in mass due to cryogen evaporation and refill. With access only available from above, there are several possible means of bringing the high-intensity pulsed laser light into the active region of the NMR probe.

1. Fused silica light pipes

Fused silica light pipes are an expensive and fragile solution that would require complete removal of the section of light pipe inside the magnet bore every time the sample was changed. Silica rods decollimate the light and are prone to gradual deterioration under intense UV light, forming cracks and "snow" along the beam path. Because of their rigidity, light pipes are an unattractive option since the vertical position of the magnet may change by as much as a few centimeters during a cryogen evaporation/refill cycle.

2. Liquid light guides

In evaluating this option we found the decollimation and optical power loss (at 355 nm) in a 5 m length of a liquid light guide to be unacceptable. The fused silica terminal windows of the light guide suffer the same kind of damage as solid silica light pipes. Furthermore, the iron alloy ferrules on most liquid light guides are incompatible with the superconducting magnet, and bespoke ferrules tend to be expensive. Liquid light guides are also insufficiently flexible and quite heavy, making it difficult to position a sample tube attached to a light guide inside the magnet bore.

3. Optical fibers and fiber bundles

Attempts to send a 10 ns, 100 mJ UV light pulse through a single optical fiber of any diameter usually result in destruction of the fiber. Fiber bundles terminated by large diameter fused silica rods were also considered, but were ruled out for cost reasons.

4. Through-air delivery using prisms and/or mirrors

This was found to be the most satisfactory and cost-effective option. Three fused silica prisms or 355 nm dichroic mirrors and one long-focus fused silica lens are required to route the light to the sample and reduce the beam diameter from 8 mm at the laser aperture to 4 mm at the sample entrance (see a detailed description below).

B. NMR sample considerations

In a typical photo-CIDNP experiment it is often a requirement that the NMR sample is deoxygenated and isolated from the atmosphere.[3] Sample tubes can be kept airtight by inserting a short, tightly fitting quartz rod, extending from the mouth of the tube to the coil region, which acts simultaneously as a light guide.[19] Alternatively, a smaller diameter D_2O-filled NMR tube placed inside the sample tube can fulfill the same role. With the latter we found it difficult to reproduce the optical power that reached the sample due to variable light scattering at the water meniscus. Fused silica rods, 20 cm long and 4 mm in diameter, with optically polished ends were therefore preferred. These are easily replaced if substantial photodamage occurs, and with cylindri-

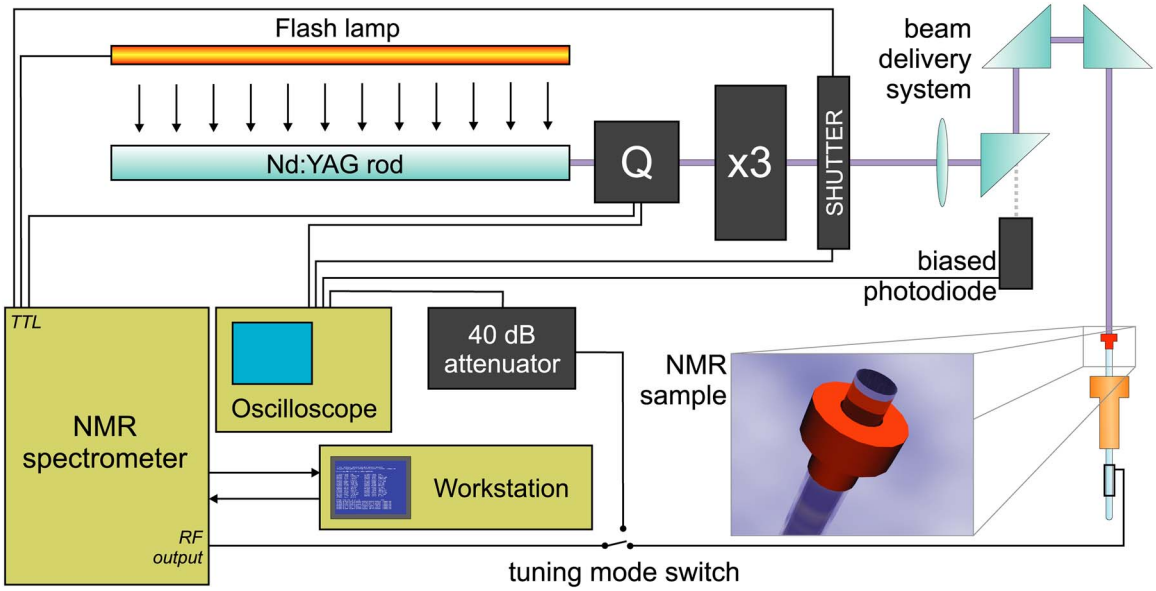

FIG. 1. (Color online) Block diagram of the time-resolved photo-CIDNP experiment using a frequency-tripled (355 nm) Nd:YAG laser and sample illumination from above (to avoid the necessity for NMR probe modifications). The lamp, the Q switch (Q) and the optional safety interlock shutter are controlled by the spectrometer via built-in TTL lines triggered from within the pulse sequence with event timing accuracy monitored on the oscilloscope. The beam-delivery system comprises frequency mixing crystals ($\times 3$), a long-focus silica lens and either three 355 nm dichroic mirrors or three fused silica prisms; the light is directed to the NMR sample from above through the magnet bore. A 4 mm diameter fused silica rod is used both to guide light to the active region of the sample and to isolate the sample from the atmosphere.

cally shaped rods, the bubbles that tend to form between the solution layer and the lower end of the rod can be expelled without difficulty.

C. Laser operation and synchronization

Pulsed gas (e.g., excimer) lasers—extensively used in the past for time-resolved CIDNP experiments[14,24,28]—are convenient in that they do not require an extended warmup period to obtain a reproducible output, but are problematic due to their poor collimation and large beam cross section. Doped YAG lasers, on the contrary, have excellent collimation, but require an extended warmup period with the necessity to flash the lamp repetitively to achieve a stable optical output. Since efficient light routing is the primary concern, a frequency-tripled Nd:YAG laser was chosen as the light source in the hardware described below. The continuous lamp operation and the synchronization of the Q switch and the rf pulse sequence turned out to be straightforward to implement in software.

III. HARDWARE ARRANGEMENT AND OPERATION

Our time-resolved photo-CIDNP setup is shown schematically in Figs. 1 (block diagram) and 2 (geometric layout). The Varian Inova 600 NMR spectrometer has five spare TTL lines that can be triggered from within the pulse sequence, allowing convenient control of external equipment. The arrangement described here uses three lines, two of which trigger the lamp and the Q switch of the Nd:YAG laser; the third controls the optional safety interlock shutter. The required synchronization accuracy ($\sim$100 ns) is easily met by the built-in TTL lines of both spectrometer and laser.

The beam delivery system may contain two or three deflectors (either prisms or mirrors). The two-prism configuration (without Prism B, Fig. 2), requiring the beam to be sent at an oblique angle across the room, was ruled out on safety grounds. A three-prism configuration was therefore implemented. Prism A sends the beam vertically towards the ceiling, where prism B directs it horizontally, well above eye-level, to a position above the magnet. Prism C, mounted exactly above the center of the magnet bore, sends the beam downwards towards the sample. Ideally, all prisms need X,Y,Z translation and θ,ϕ rotation stages to facilitate alignment.

At 355 nm, prisms have the advantage of being less expensive than high-energy dichroic mirrors, but each prism

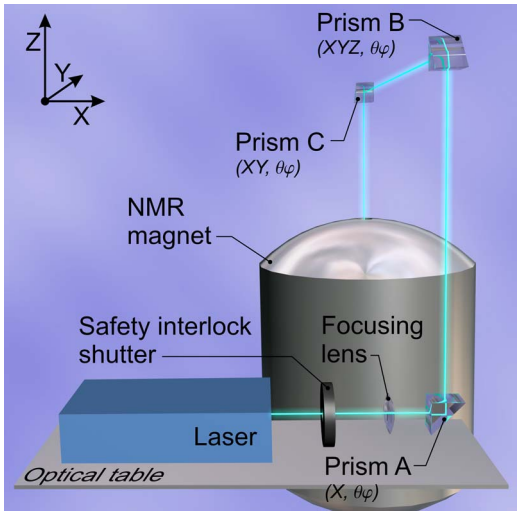

FIG. 2. (Color online) Schematic drawing of the spatial hardware arrangement for the time-resolved photo-CIDNP experiment. Ideally, all three deflectors (prisms or mirrors) should have full rotation and translation stages to facilitate alignment. Minimum requirements for the degrees of freedom are shown in the picture.

results in a ~10% optical power loss due to light scattering at its surfaces. A prism-based light routing system almost inevitably has some stray reflections, which may be put to good use by placing a prebiased fast photodiode into the path of the stray beam and using the resulting signal to check the timing accuracy of the experiment. The pulse widths and timings specified in the pulse sequence were found to be reproduced by the Inova 600 hardware with an apparent accuracy of better than 10 ns.

Alignment of the beam with respect to the sample may be achieved by putting an empty NMR tube plus spinner in the magnet, removing the probe, and maximizing the signal from a photodiode placed coaxially beneath the magnet. A frosted glass plate in the beam path just above the photodiode ensures that it reports the overall light amplitude rather than accidental focusing spots generated by the bottom of the NMR tube. The minimum requirements for the degrees of freedom of the three prisms or mirrors are given in Fig. 2. Once the arrangement has been set up, only prism C needs regular (every few days) adjustment, a consequence of small magnet movements arising from cryogen evaporation. Seasonal changes in the geometry of the building may occasionally (once every few months) make it necessary to adjust prisms A and B. It is convenient to monitor the beam position at the sample entrance using a paper collar placed around the quartz rod. Burn marks on the collar indicate the need for realignment.

The lens (at least 5 m focal length was found to be required in practice) may be mounted anywhere along the beam path, the most convenient location being the optical table. Care must be taken to avoid focusing the beam to a point anywhere along its trajectory. If the beam diameter is reduced below 3 mm, snow-like lesions usually form within the fused silica optical components, resulting in a degraded performance. The beam must also pass far enough from the volume accessible to spectrometer users to comply with safety regulations, which have also imposed a need to black out the windows of the spectrometer room with opaque material.

In our experience, acceptable magnetic field homogeneity can only be achieved if the lower end of the quartz rod is positioned at least 1 mm (up to 3 mm for very high resolution work) above the top of the receiver coil. This means that there is an absorptive layer of solution between the tip of the rod and the active region which attenuates the light, To maximize the sensitivity, the sample concentration would normally be adjusted for maximum light utilization, as outlined below.

Assuming that the laser light comes uniformly from above, the amount of laser light absorbed in the active NMR sample volume is

$$I_{\mathrm{abs}} = I_0(1 - 10^{-\epsilon c \ell})10^{-\epsilon c d}, \tag{1}$$

where c is the photosensitizer concentration, ℓ is the coil length, d is the height of the liquid between the end of the quartz rod and the top of the coil, I_0 is the amount of laser light emerging from the quartz rod, and ϵ is the extinction coefficient of the photosensitizer. Finding the maximum of I_{abs} with respect to the photosensitizer concentration for given ℓ, d, and ϵ yields the optimum concentration c_{opt}

$$c_{\mathrm{opt}} = \frac{1}{\epsilon \ell}\log\left(1 + \frac{\ell}{d}\right). \tag{2}$$

Back substitution of Eq. (2) into Eq. (1) gives the maximum fraction of the light that is absorbed productively

$$f_{\max} = \frac{I_{\mathrm{abs}}(c_{\mathrm{opt}})}{I_0} = \frac{1}{1 + d/\ell}\left(1 + \frac{\ell}{d}\right)^{-d/\ell}. \tag{3}$$

The quantity $f_{\max}$ has been is plotted in Fig. 3 for a $\ell = 16$ mm coil, and $d = 1$ mm (solid line), and $d = 2$ mm (dashed line), and $d = 3$ mm (dotted line). This treatment allows one to choose the optimal photosensitizer concentration to ensure maximum utilization of the incident light.

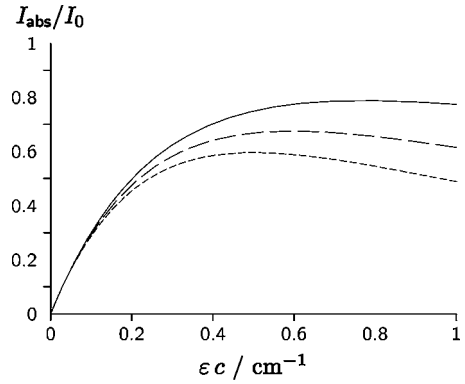

FIG. 3. Plot of Eq. (3) for a 16 mm NMR coil and $d = 1$ mm (solid line), $d = 2$ mm (dashed line), and $d = 3$ mm (dotted line).

IV. SOFTWARE DESCRIPTION

A basic time-resolved CIDNP pulse sequence for a Nd:YAG laser is shown in Fig. 4. The lamp and Q switch are controlled using the spare TTL lines, triggered from within the pulse sequence. The requirement to keep the lamp running at a constant repetition rate results in the relaxation delay being replaced by a series of n lamp cycles, with the delay τ_{r} being the reciprocal of the laser repetition frequency. The penultimate lamp cycle contains a background signal suppression scheme aligned to the end of the cycle. For this purpose, we have used a series of 3–5 90° pulses followed by pulsed field gradients. The degree of suppression of unwanted NMR signals can be improved by using composite 90° pulses designed to minimize residual z magnetization.[29] The suppression sequence is followed by a lamp flash and, after a population inversion period (labeled τ_{pi}, typically

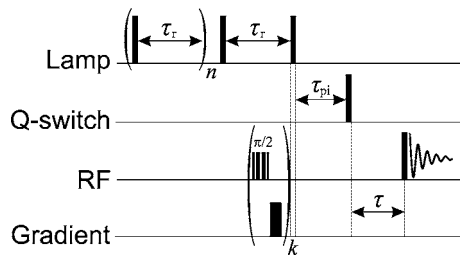

FIG. 4. Simple time-resolved photo-CIDNP pulse sequence written specifically to allow the Nd:YAG laser lamp to run continuously throughout the experiment. The radio frequency pulses preceding the gradients are 45-90-90-45 composite pulses.

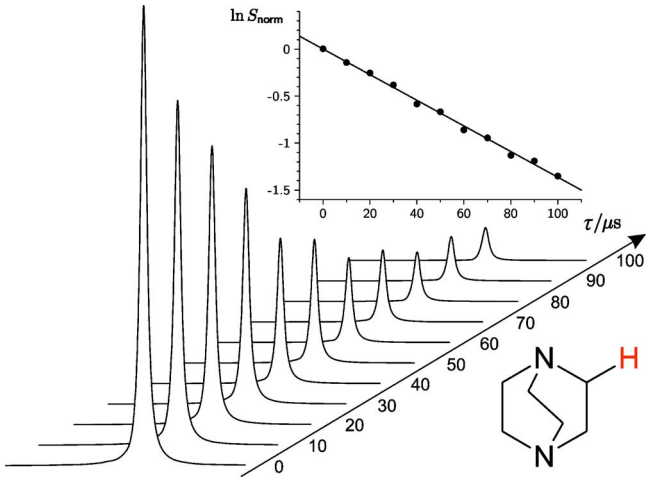

FIG. 5. (Color online) ^{1}H photo-CIDNP kinetics in the DABCO/FMN reaction. The signal belongs to the twelve equivalent protons of DABCO.

150–180 μs), the Q switch is triggered. The light pulse (5–10 ns) follows after about 50 ns, the time taken for the Q switch to respond to the TTL voltage ramp. After the light pulse, an incremented period τ is introduced, during which the photochemical reaction proceeds. The magnetization is then sampled by the rf pulse, which must be as short as possible (for the best time resolution) and at the same time as close as possible to 90° (for optimum sensitivity). A reasonable compromise for a typical photo-CIDNP experiment is a 1.0 μs observation pulse at full available (or permissible, depending on the probe capacitor damage threshold) rf amplifier power. Given sufficient signal-to-noise ratio, the time resolution can be increased by deconvolution or iterative reconvolution.[30]

While Fig. 4 represents all the essential parts of the pulse sequence for time-resolved photo-CIDNP, it is important to realize that commercial pulse sequence programming languages contain multiple "hidden" (but well-documented) delays in their pulse statements. These may be as large as several tens of microseconds and may be different for different amplifiers, probes, and nuclei. This means that all the time-critical statements should be coded explicitly to avoid ambi-

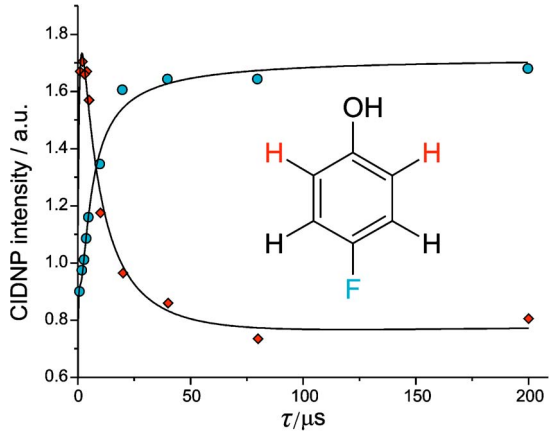

FIG. 6. (Color online) ^{1}H (diamonds) and ^{19}F (circles) photo-CIDNP kinetics in the 4-fluorophenol/FMN reaction. The solid lines represent the theoretical best fit using the model suggested by Vollenweider and Fischer (see Ref. 4).

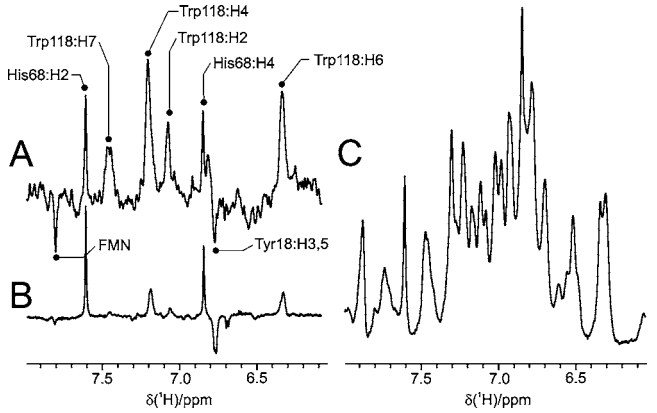

FIG. 7. The aromatic regions of ^{1}H spectra of calcium-depleted bovine α-lactalbumin with FMN photosensitizer in D_2O buffered by sodium cacodylate at pH 7.7. (a) Time-resolved ^{1}H photo-CIDNP spectrum (τ=0) recorded. (b) Continuous-wave ^{1}H photo-CIDNP spectrum obtained using an Ar^+ laser as the light source (100 ms light flash at 488 nm with 15 W output power). (c) Conventional ^{1}H NMR spectrum. Spectra (a) and (b) show the difference between the illuminated and the "dark" spectrum with all other settings kept the same.

guities. In particular, the amplifier unblanking delay which precedes the rf pulse must be constant to ensure that the pulse power is stable. The length of this period for modern amplifiers is about 10 μs, meaning that when the τ delay passes the 10 μs mark, the unblanking delay and the preceding Nd:YAG population inversion delay need to be appropriately reordered in the software.

V. EXAMPLES

Examples of the magnetokinetic data and time-resolved CIDNP spectra recorded with the pulse sequence of Fig. 4 are shown in Figs. 5–7. After the laser flash, the geminate radical pair spin-sorting process is finished in the first few hundred nanoseconds. The detected magnetization dynamics is therefore due to the magnetic and chemical transformations in those radicals that have escaped the primary cage recombination.[1] The particular case of a dye-sensitized pulsed photo-CIDNP experiment has been treated by Vollenweider and Fischer[4,5] who suggested the following system of equations to describe the kinetics of the escaped radicals and the associated nuclear polarizations:

$$R(t) = \frac{R_0}{1 + k_t R_0 t}$$

$$\frac{dP}{dt} = -k_t PR - k_t \beta R^2 - \frac{P}{T_1} - k_{ex} CP \qquad (4)$$

$$\frac{dQ}{dt} = k_t PR + k_t \beta R^2 + k_{ex} CP.$$

The first equation in Eq. (4) gives the concentration of the escaped radicals which are assumed to recombine with second order kinetics, with equal initial concentrations of donor cations and photosensitizer anions, $[A^+](0)=[F^-](0)=R_0$, and a second order termination rate constant k_t:

$$\begin{aligned} &\mathrm{F} \xrightarrow{h\nu} {}^1\mathrm{F} \rightarrow {}^3\mathrm{F} \\ &\mathrm{A} + {}^3\mathrm{F} \rightarrow \mathrm{A}^{\cdot+} + \mathrm{F}^{\cdot-} \\ &\mathrm{A}^{\cdot+} + \mathrm{F}^{\cdot-} \xrightarrow{k_t} \mathrm{A} + \mathrm{F} \\ &\mathrm{A}^{\cdot+} + \mathrm{A} \xrightarrow{k_{ex}} \mathrm{A} + \mathrm{A}^{\cdot+}. \end{aligned} \tag{5}$$

The second and third equations describe the magnetization of a given nucleus in the pool of radicals (P) and diamagnetic molecules (Q) with the first term describing recombination in singlet encounters and the second describing F-pair encounters that generate additional magnetization, specified by the factor $\beta=\gamma P^G/R_0$. The nuclear paramagnetic relaxation in the escaped radicals is assumed to be described by a single characteristic time T_1. The last terms of the second and third equations describe the transfer of magnetization between radicals and their diamagnetic parent molecules present at concentration C by degenerate electron exchange with a rate constant, k_{ex}. The initial conditions for the magnetizations, $P(0)=-P^G, Q(0)=P^G$, reflect the spin-sorting nature of the radical pair mechanism, where the initial polarization (P^G) must be exactly opposite in geminate recombination products and escaped radicals.[1]

Although the solution to Eqs. (4) does exist in a closed algebraic form, the fastest way to solve and fit them to the experimental data nevertheless appears to be numerical. The abundance of variable parameters in Eqs. (4) often necessitates global fitting of data sets in which, for example, the electron donor concentration is varied systematically.[31] Optionally, the initial guess may be first refined using a numerically efficient (4,4) Padé approximant[32] around $t=0$, which approximates the solution of Eqs. (4) to within about 3% within the operational interval. Starting the full minimization from this refined guess reduces the computation time by about one order of magnitude.

In the case of the photochemical reaction of the electron donor 1,4-diazabicyclo(2.2.2)octane (DABCO) with the photosensitizer flavin mononucleotide (FMN) (Fig. 5) the dominant mechanism of magnetization transfer between the escaped radicals and the diamagnetic products is degenerate electron transfer,[33] meaning that the $k_{ex}CP$ term in Eqs. (4) dominates. The result is pseudofirst order magnetization kinetics and hence an exponential decay in the nuclear polarization, Q, and the nearly perfect cancellation of the geminate and escape polarization at long time delays (Fig. 5, inset). In this particular case, the degenerate electron transfer rate constant was determined to be 8.0×10^6 M^{-1} s^{-1}.[34]

The magnetization dynamics for the 4-fluorophenol/FMN reaction (Fig. 6) do not involve degenerate electron transfer due to rapid deprotonation of the initially formed phenol cation radical, so that the $k_{ex}CP$ term can be dropped from Eqs. (4). The initial sharp rise of both proton and fluorine signals is due to magnetization generation in F-pairs.[1] It is followed by either a plateau (fluorine) or partial bulk recombination cancellation (protons). The lack of magnetization cancellation in the case of the ^{19}F nuclei is due to their extremely efficient spin-lattice relaxation in the phenoxyl radical caused by the large hyperfine coupling anisotropy.[32] Fitting Eqs. (4) to these data results in proton and fluorine T_1 values of 56 and 0.13 μs, respectively. Such parameters would be difficult to measure by other means for such a short-lived radical.[22]

Figure 7 shows the aromatic region of the 600 MHz ^{1}H photo-CIDNP (A, B) and NMR (C) spectra obtained for calcium-depleted bovine α-lactalbumin (1.5 mM) with FMN photosensitizer (80 μM) in the presence of 50 mM sodium cacodylate buffer at pH 7.7 (in D_2O, uncorrected for deuterium isotope effect). In the case of the time-resolved spectrum [Fig. 7(a)] the magnetization was sampled and acquired immediately after the light pulse to avoid secondary out-of-cage photochemical reactions[1] and so to ensure that only geminate CIDNP is present.[23,34] This geminate polarization is directly related to the accessibility to the bulk solvent of the highest occupied molecular orbital of the aromatic amino acid residue and in principle allows a quantitative interpretation of CIDNP intensities in terms of side-chain solvent accessibilities. This would be difficult to do with steady-state CIDNP [Fig. 7(b)] because of distortions caused by the secondary magnetization dynamics (an example of which is given in Fig. 6) and diamagnetic cross-relaxation occurring on the timescale of the steady-state photo-CIDNP experiment. As one can see from comparing Figs. 7(a) and 7(b) the secondary processes introduce significant intensity changes and preclude simple quantitative analysis. The conclusion in this particular case is that the Trp118, His68, and Tyr18 residues are sufficiently exposed to the solvent for electron transfer (Tyr, Trp) or hydrogen atom transfer (His) to occur to the photosensitizer, with a rather low solvent exposure for Tyr18. A consideration of solvent accessibilities based on the steady-state photo-CIDNP spectrum [Fig. 7(b)] would have overestimated the accessibility of Tyr18 and strongly underestimated that of Trp118. Another notable phenomenon which is absent from the cw CIDNP spectrum is the fact that the H(7) proton of the tryptophan aromatic ring shows a substantial geminate CIDNP polarization, indicating that, contrary to PCM solvent *ab initio* calculations of tryptophan radicals[32] and in agreement with *in situ* protein electron phonon resonance data,[35] H(7) does have a hyperfine coupling of at least 0.3 mT in the intermediate tryptophan radicals of a protein/FMN reaction system.

ACKNOWLEDGMENTS

Financial support from the BBSRC and INTAS (Project No. 02-2126) and the DFG (Grant Nos. Go615/6-3 and Go615/9-1) is gratefully acknowledged. I.K. thanks the Scatcherd European Foundation and the Hill Foundation for a PhD studentship.

[1] L. T. Muus, P. W. Atkins, K. A. McLauchlan, and J. B. Pedersen, *Chemically Induced Magnetic Polarization: Proceedings of the NATO Advanced Study Institute*, Sogesta, Urbino, Italy, April 17-30, 1977 (Reidel, Dordrecht, 1977).
[2] M. Goez, Adv. Photochem. **23**, 63 (1997).
[3] K. M. Salikhov, Yu. N. Molin, and A. L. Buchachenko, *Spin Polarization and Magnetic Effects in Radical Reactions* (Elsevier, New York, 1984).
[4] J. K. Vollenweider and H. Fischer, Chem. Phys. **124**, 333 (1988).
[5] J. K. Vollenweider, H. Fischer, J. Hennig, and R. Leuschner, Chem. Phys.

97, 217 (1985).
[6] P. J. Hore and R. W. Broadhurst, Prog. Nucl. Magn. Reson. Spectrosc. **25**, 345 (1993).
[7] R. Kaptein, Biol. Magn. Reson. 4, 145 (1982).
[8] R. Kaptein, K. Dijkstra, and K. Nicolay, Nature (London) **274**, 293 (1978).
[9] T. Kuhn and H. Schwalbe, J. Am. Chem. Soc. **122**, 6169 (2000).
[10] J. Wirmer, T. Kuhn, and H. Schwalbe, Angew. Chem. **40**, 4248 (2001).
[11] P. Wenter, B. Fuertig, A. Hainard, H. Schwalbe, and S. Pitsch, Angew. Chem. **44**, 2600 (2005).
[12] P. J. Hore, E. R. P. Zuiderweg, R. Kaptein, and K. Dijkstra, Chem. Phys. Lett. **83**, 376 (1981).
[13] O. B. Morozova, Yu. P. Tsentalovich, A. V. Yurkovskaya, and R. Z. Sagdeev, J. Phys. Chem. A **102**, 3492 (1998).
[14] O. B. Morozova, A. V. Yurkovskaya, Yu. P. Tsentalovich, M. D. E. Forbes, P. J. Hore, and R. Z. Sagdeev, Mol. Phys. **100**, 1187 (2002).
[15] S. M. Harper, L. C. Neil, I. J. Day, P. J. Hore, and K. H. Gardner, J. Am. Chem. Soc. **126**, 3390 (2004).
[16] S. M. Harper, L. C. Neil, and K. H. Gardner, Science **301**, 1541 (2003).
[17] G. Rubinstenn, G. W. Vuister, F. A. A. Mulder, P. E. Dux, R. Boelens, K. J. Hellingwerf, and R. Kaptein, Nat. Struct. Biol. **5**, 568 (1998).
[18] G. Rubinstenn, G. W. Vuister, N. Zwanenburg, K. J. Hellingwerf, R. Boelens, and R. Kaptein, J. Magn. Reson. **137**, 443 (1999).
[19] P. W. Atkins, J. M. Frimston, P. G. Frith, R. C. Gurd, and K. A. McLauchlan, J. Chem. Soc., Faraday Trans. 2 **69**, 1542 (1973).
[20] I. Kuprov and P. J. Hore, J. Magn. Reson. **171**, 171 (2004).
[21] J. E. Scheffler, C. E. Cottrell, and L. J. Berliner, J. Magn. Reson. (1969-1992) **63**, 199 (1985).
[22] I. Kuprov and P. J. Hore, J. Magn. Reson. **168**, 1 (2004).
[23] M. Goez, Concepts Magn. Reson. **7**, 263 (1995).
[24] R. J. Miller and G. L. Closs, Rev. Sci. Instrum. **52**, 1876 (1981).
[25] B. Blank, A. Henne, and H. Fischer, Helv. Chim. Acta **57**, 920 (1974).
[26] A. V. Yurkovskaya (personal communication).
[27] G. G. McDonald, J. Magn. Reson. (1969-1992) **53**, 115 (1983).
[28] A. V. Yurkovskaya, O. B. Morozova, R. Z. Sagdeev, S. V. Dvinskih, G. Buntkowsky, and H. M. Vieth, Chem. Phys. **197**, 157 (1995).
[29] R. R. Ernst, G. Bodenhausen, and A. Wokaun, *Principles of Nuclear Magnetic Resonance in One and Two Dimensions* (Clarendon, New York, 1987).
[30] M. Goez, Chem. Phys. Lett. **165**, 11 (1990).
[31] Yu. P. Tsentalovich, O. B. Morozova, A. V. Yurkovskaya, and P. J. Hore, J. Phys. Chem. A **103**, 5362 (1999).
[32] I. Kuprov, PhD thesis, University of Oxford, 2005.
[33] H. D. Roth and A. A. Lamola, J. Am. Chem. Soc. **96**, 6270 (1974).
[34] O. B. Morozova, A. V. Yurkovskaya, R. Z. Sagdeev, K. H. Mok, and P. J. Hore, J. Phys. Chem. B **108**, 15355 (2004).
[35] F. Lendzian *et al.* J. Am. Chem. Soc. **118**, 8111 (1996).